

Tip-Enhanced Raman Spectroscopy of Cell Wall Heterogeneity for *Aspergillus Fumigatus*

Zhenfei Jiang^{1,2,†}, Jizhou Wang^{1,†}, Zhe He^{3,*}, Peng Zhang³, Zhenhuan Yi^{1,2}, Alexei V. Sokolov^{1,2,4}, Marlan O. Scully^{1,2,5}

¹*Institute for Quantum Science and Engineering, Texas A&M University, College Station, TX 77843, USA*

²*Department of Physics and Astronomy, Texas A&M University, College Station, TX 77843, USA*

³*Shandong Institute of Advanced Technology, Jinan, Shandong, China*

⁴*Department of Electrical and Computer Engineering, Texas A&M University, College Station, TX 77843, USA*

⁵*Department of Electrical and Computer Engineering, Princeton University, Princeton, NJ 08540, USA*

†These authors contribute equally.

*Corresponding author: zhe.he@iat.cn

Abstract: Tip-enhanced Raman spectroscopy (TERS) enables nanoscale chemical mapping of biological structures, providing high-resolution, high-signal-to-noise ratio imaging into molecular distribution and interactions beyond the capabilities of conventional Raman imaging. However, challenges such as the deformation of fragile biological cells and the complexity of signal interpretation would increase the difficulty in investigating biological samples with TERS. Here, we demonstrate using TERS to investigate the cell wall heterogeneity of *Aspergillus fumigatus* spores. Using TERS imaging and spectral analysis, we map the chemical components including melanin within the fungal cell wall. The results reveal distinct spectral features associated with polysaccharides, lipids, and proteins. Furthermore, by comparing the wild-type and albino mutant spores, we illuminate the biochemical characteristics of Dihydroxynaphthalene melanin (DHN-melanin) in the fungal cell wall.

I. INTRODUCTION

Tip-enhanced Raman spectroscopy (TERS) combines Raman spectroscopy with scanning probe microscopy (SPM), which enhances traditional Raman spectroscopy by providing nanoscale spatial resolution and single-molecule sensitivity. TERS relies on the field enhancement effect of a metallic tip, typically made of silver or gold. This

enhancement is primarily driven by the localized surface plasmon resonance (LSPR), generating a hotspot of the local electromagnetic fields. The intense field amplifies the Raman signal of molecules in proximity to the size of the tip. Therefore, by scanning the tip across a sample, TERS enables sensitive Raman spectroscopy within a nanoscale volume, down to sub-nanometer level¹⁻⁴.

Based on the high sensitivity and super-resolution capability, TERS has been used to study the chemical components of a single molecule such as DNA and protein^{5,6}, as well as small viral particles⁷. However, challenges remain for applying TERS to cellular imaging. The irregular surface topography and bulky structure of cells hinder the gap-mode TERS, which is extensively employed in bio-sensing, thereby limiting the imaging sensitivity. As a result, imaging a cell typically demands higher laser power compared to single-molecule imaging, increasing the risk of thermal damage induced by LSPR of the tip. In terms of fungal cells, the soft nature of the cell wall reduces the stability of tip contact. Additionally, the heterogeneous chemical composition of the cell wall limits the reproducibility of TERS scans. In this study, we explore the application of TERS on fungal cell walls, highlighting the complex distribution of components, especially the melanin clusters.

Melanin, a negatively charged molecule, is usually observed in the fungal cell wall as layers of globular particles⁸⁻¹⁰. It protects the fungus against external impact, such as UV radiation and oxidative damage. In 1998, Tsai *et al.* have investigated the albino mutant (*alb1*) gene in *Aspergillus fumigatus*, focusing on its impact on spore morphology and fungal virulence¹¹. The *alb1* gene plays an important role in the pigmentation of conidia, which is essential for their protection against stress and immune evasion. Mutations in the *alb1* gene lead to changes in conidial color, morphology, and reduced virulence, making the fungus more vulnerable to immune defenses.

In this work, we map the chemical distribution of the wild-type *A. fumigatus* and the albino mutant (*alb1*) spores. We demonstrate a technique for non-invasive TERS imaging of fungal cell walls and detail the strategies to achieve high-resolution mapping. Additionally, we provide a comprehensive peak assignment for the TERS spectra of *A. fumigatus* spores. This work reveals the biochemical characteristics of melanin composition, and the biochemical changes associated with the *alb1* gene mutation in *A. fumigatus*.

II. MATERIALS AND METHODS

The schematic of the TERS experiments is shown in Fig. 1. The samples are placed on an X-Y translation stage integrated with an atomic force microscope (AFM) coupled to an Electron-multiplying CCD (EMCCD) spectrometer (Horiba). A silicon AFM tip is used to acquire standard-resolution AFM images of spores. Subsequently, a silver-coated tip is utilized for TERS imaging. We set the scanning rate to 0.2 Hz to

ensure enough time to navigate the tip across the spores during measurements. The AFM scanning process is conducted in tapping mode to minimize interaction forces, while the subsequent TERS imaging employs contact mode to generate a hotspot at the target area. A 660 nm pump laser is focused through a 100× objective lens on the tip. The LSPR on the tip forms a hotspot at the bottom, with an area $A_{NF} = \pi(d_{tip}/2)^2$ ¹², around 0.002 μm^2 . This is remarkably smaller compared to the far-field area ($A_{FF} \sim 1 \mu\text{m}^2$), resulting in super-resolution imaging^{1,13}.

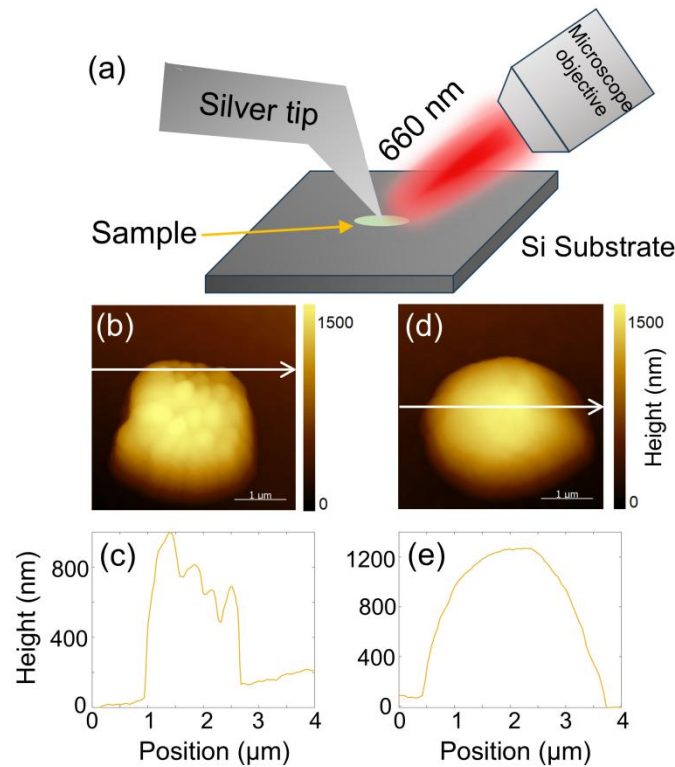


Figure 1 AFM images of *Aspergillus Fumigatus* and *alb1*. **a**, schematic of TERS. The solution of wild-type *A. fumigatus* is dropped on a silicon (Si) substrate. An objective (100×, NA 0.7) is used to focus the 660 nm laser on the tip and collect backscattered light. **b**, AFM image of a wild-type *A. fumigatus* spore. **c**, height profile along the arrow in **(b)**. The bumpy curve shows the shape of melanin within the spore. **d**, AFM image of the albino mutant (*alb1*) of *A. fumigatus* spore that lacks melanin. **e**, height profiles along the arrow in **(d)**.

Figure 1b displays the AFM image of a wild-type *A. fumigatus* spore, while Fig. 1c shows the corresponding height profiles along the arrow in Fig. 1b. The arrow at the edge is selected to show a clear bumpy profile of the melanin particles. The size of melanin is around 300 nm, which is much smaller compared to the spore. The AFM image of *alb1* spore is provided in Fig. 1d, and the height profiles along the arrow are presented in Fig. 1e. The height of the *alb1* spore is approximately 1.3 μm . The shape of the spore is usually ellipsoid due to gravity, the measured width is about 3 μm .

III. EXPERIMENTAL RESULTS

The confocal Raman imaging and selected spectral analysis of an *alb1* mutant spore are presented in Fig. 2. Figure 2a shows the confocal Raman image. The color bar shows the intensity integrated over the Raman signal from 1120 cm^{-1} to 1800 cm^{-1} . Figure 2b displays four Raman spectra, each obtained from selected positions within the spore. The positions are labeled by crosses in Fig. 2a, respectively. The detailed assignment of the peaks is provided in Table 1.

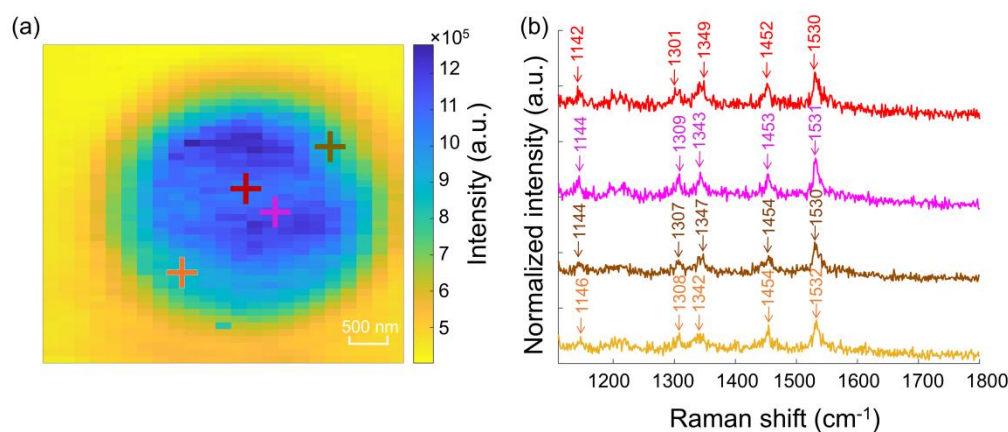


Figure 2 Raman spectroscopy of an *alb1* spore. **a**, confocal Raman imaging. The intensity at each point is integrated over the Raman spectra from 1120 cm^{-1} to 1800 cm^{-1} . The acquisition time at each point is 0.5 seconds. The scanning step size is 100 nm. **b**, Raman spectra at the labeled positions of an *alb1* spore in **(a)**. Red and purple curves: Raman signals near the central area of the *alb1* spore. Brown and orange curves: Raman signal near the edge area of the *alb1* spore. The positions are labeled by crosses in **(a)** with corresponding colors, respectively.

Table 1 Raman peak assignments for spectra in Fig. 2.

Approximate Wavenumber Range (cm^{-1})	Peak Assignment
1142~1146	C-O and C-C stretching vibrations in polysaccharides ^[14]
1301~1309	vibrational modes associated with CH_2 and CH_3 deformation in proteins and lipids ^[11, 15]
1342~1349	the C-H bending vibrations of aliphatic groups ^[14, 15]
1452~1454	CH_2/CH_3 deformations or bending modes found in lipids and proteins ^[15]
1530~1532	molecular vibrations related to aromatic ring structures or C=C stretching ^[16, 17]

In Fig. 2, confocal Raman spectra of the *alb1* mutant of *A. fumigatus* reveal a homogeneous biochemical composition. The major peaks that fingerprint the *alb1* spore are marked. The 1144 cm^{-1} peak is related to C-O and C-C stretching vibrations in polysaccharides such as β -glucans, contributing to the structural integrity and

hydrophilicity of the cell wall¹⁴. The 1307 cm^{-1} and 1453 cm^{-1} peaks are associated with CH_2/CH_3 deformations in proteins and lipids^{11,15}. Additionally, the 1342 cm^{-1} peak is likely associated with the C-H bending vibrations of aliphatic groups^{14,15}. The 1530 cm^{-1} peak is related to the aromatic ring structure, which shows a typical peak observed in biomaterials^{16,17}.

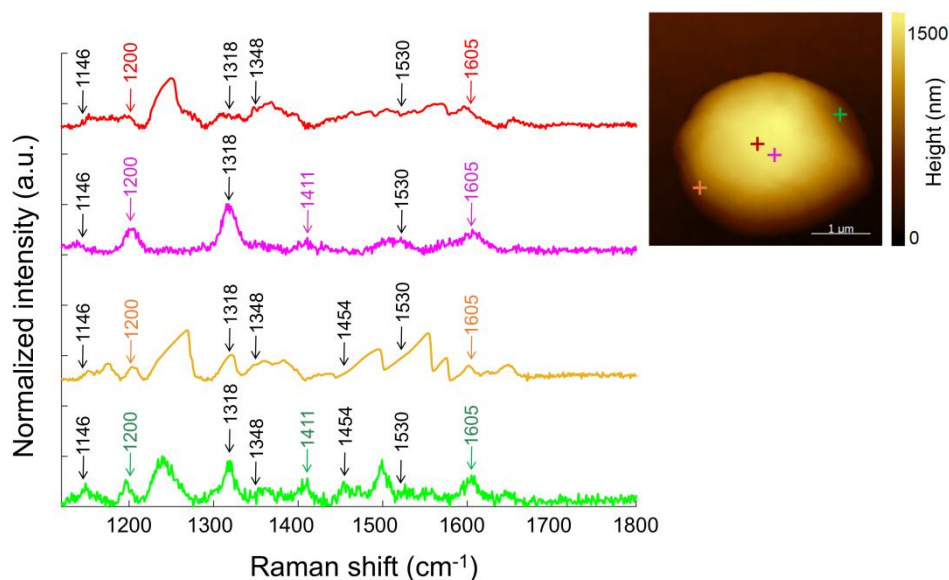


Figure 3 TERS signals from 1120 cm^{-1} to 1800 cm^{-1} for selective points on an *alb1* spore. The acquisition time at each point is 10 seconds. Red and purple curves: TERS signal at the central area of *alb1* spore labeled by the red and purple crosses in the AFM map. Green and orange curves: TERS signal at the edge area of *alb1* spore labeled by the green and orange crosses in the AFM map. The inset at the upper right corner shows the AFM map of the *alb1* spore.

Compared to confocal imaging, TERS can resolve the localized chemical and structural information of the fungal spore. As shown in Fig. 3, some typical TERS spectra of the *alb1* spore indicate heterogeneity across the spore, which cannot be observed with the confocal Raman microscope. For instance, the TERS signals from the central region of the spore (red and purple curves) are diverse, highlighting the presence of localized differences even between closely positioned areas. Moreover, the TERS signals obtained from opposite edges of the spore (green and orange curves) exhibit even greater differences, further emphasizing the heterogeneity of the *alb1* spore cell wall.

Specific TERS peaks in the range of 1120 cm^{-1} to 1800 cm^{-1} are labeled in Fig. 3. In addition to peaks already present in conventional Raman spectra, TERS enhances and modifies the spectral intensity. For example, the peak at 1200 cm^{-1} attributed to polysaccharide vibrations essential for the structural integrity of the fungal cell wall^{11,15,16,18,19}, is only weakly visible in conventional Raman spectra (Fig. 2b); however, TERS substantially enhances this peak. Furthermore, peaks at 1411 cm^{-1}

and 1605 cm^{-1} , which are almost undetectable in Fig. 2b, are clearly identified through TERS. Additionally, TERS induces spectral shifts. For instance, the 1318 cm^{-1} peak in Fig. 3, attributed to C-H bending vibrations^{11,15,20}, exhibits a shift relative to the corresponding 1309 cm^{-1} peak observed in conventional Raman spectra.

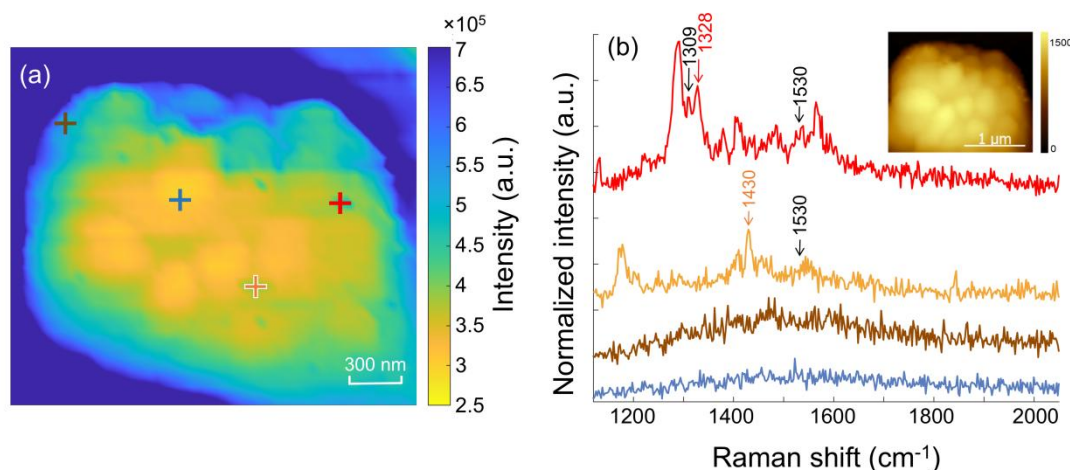


Figure 4 TERS measurement of a wild-type *A. fumigatus* spore. **a**, TERS imaging. The intensity at each point is the integrated intensity of the TERS signal from 1120 cm^{-1} to 2050 cm^{-1} . The acquisition time is one second. The step size of the scan is 50 nm . **b**, typical TERS signals selected from certain areas of the *A. fumigatus* spore in (a). Each curve is an average of the adjacent positions around the crosses in (a). Red and orange curves: the positions that are uncovered by melanin. Blue curve: the area covered by melanin. Brown curve: the edge area of the spore. The inset shows the AFM imaging of (a), which is a zoom-in area in Fig. 1(b).

Furthermore, Fig. 4 illustrates TERS imaging and selected spectral analysis of a wild-type *A. fumigatus* spore. To identify the chemical components, four representative TERS spectra corresponding to the areas marked by crosses in Fig. 4a are presented. In Fig. 4a, the yellow-colored regions indicate the presence of melanin clusters on the spore. These melanin-rich regions exhibit relatively weaker TERS signals compared to the surrounding areas. This can be attributed to the inherently weak Raman scattering cross-section of melanin, which results in low intrinsic Raman signal intensity. Additionally, the TERS technique primarily enhances near-field Raman signals by leveraging the LSPR at the tip apex. However, due to the complex optical properties of melanin, including its strong absorption and potential quenching effects, the TERS enhancement in these regions remains limited. In contrast, the edges of the melanin clusters exhibit stronger TERS signals. This enhancement can be attributed to the influence of LSPR distribution, which is not confined to the tip apex but extends to the tip sides. At the cluster edges, the near-field coupling between the tip and the surrounding material is more favorable, leading to a more pronounced TERS enhancement. Additionally, the boundary regions may contain structural or

compositional variations that further influence the local enhancement of the Raman signal. For example, the melanin peak at 1430 cm^{-1} is only shown next to the melanin clusters. While the LSPR density on the tip side is lower compared to that at the tip apex, the larger contact area at the tip side contributes to a greater Raman enhancement, resulting in increased TERS signal intensity.

In Fig. 4b, the 1309 cm^{-1} and 1530 cm^{-1} are detected in both the wild-type spore and *alb1* spore, indicating common chemical structures. However, certain peaks highlight the presence of melanin. Here, the 1328 cm^{-1} peak is only observed in the wild-type spore, representing amide III stretching vibrations that are related to DHN-melanin, reflecting essential components of spore pigmentation and cell structure^{15,18,21,22}. Peak at 1430 cm^{-1} indicates C=C stretching vibrations of aromatic ring structures typical of melanin^{15,21–24}.

IV. DISCUSSION

Applying a scanning probe to image cells presents several challenges. One of the issues is the fragility of soft cellular structures, which can be easily compromised by the plasmon heating effects that may arise during tip contact and the mechanical forces during scanning. Moreover, the soft nature of the cell can introduce noise, resulting in reduced image contrast, which constrains the maximum feedback gain that can be employed during imaging. In our experiment, we observed that *alb1* spores are more prone to damage compared to the wild-type spores. Spores that sustain damage often exhibit strong signals, which is probably because the tip is contaminated by the cell fluid. In this case, the tip only enhances the Raman signals of the contamination and does not sense the cell wall. To avoid the damage requires optimization of both image quality and probe parameters. For optimal imaging performance, the feedback gain of the AFM is configured to 144.2. The TERS exposure time, indicating the contact duration of the tip at each scanning step, is typically limited to one second.

The choice of substrate is also important for stable TERS scanning. Commonly used substrates, such as Si/SiO₂ and gold- or silver-coated wafers, have smooth surfaces that may fail to stabilize biological cells. During the scanning process, the pressure exerted between the tip and the sample can surpass the frictional force between the sample and the substrate, potentially causing cell displacement. To address this challenge in our experiments, a Si wafer was chosen as the substrate. To further enhance sample stability, a thin layer of agarose solution was applied to the Si wafer. After drying the agarose layer, the spores were carefully placed onto the substrate. The roughness of the agarose layer effectively prevents cell movement, providing a secure platform for stable TERS scanning. To further prevent the shear force from scraping against the cell, the scanning rate for both AFM and TERS was set to 0.2 Hz.

In conclusion, the TERS analysis of *A. fumigatus* spores yield insights into the composition in the fungal cell wall. The spatially resolved chemical mapping obtained through TERS imaging has shown the distribution of polysaccharides, lipids, proteins, and melanin, which play important roles in fungal structure, metabolism, and virulence. Comparisons between the TERS spectra of the wild-type and *alb1* spores have indicated that melanin-covered cells exhibited increased resilience against damage. These findings also highlight the potential of TERS as a powerful tool for studying aggregations in cell walls. In the TERS images, the different spectra at different positions on the cell wall indicate the heterogeneity of the cell wall, which cannot be revealed via confocal spectroscopy. We demonstrate that TERS can map the melanin in the cell wall and present the Raman signal at the edge of the clusters. Furthermore, this study provides detailed Raman peak assignments to offer a view of fungal cell walls, providing a useful tool for future investigation.

ACKNOWLEDGMENTS

The sample presented in this work was provided by Prof. Xiaorong Lin at the University of Georgia. The authors thank Dr. Dmitri V. Voronine for his technical support during this work. Z. H. acknowledges the support from Taishan Scholars Program (No. tsqn202306316), Shandong Excellent Young Scientists Fund (No. 2024HWYQ-081), and the National Natural Science Foundation of China under grant No. 12404413. P. Z. acknowledges the support from China Postdoctoral Science Foundation Fund (No. 2023M742133). A. V. S. acknowledges the support from the Welch Foundation Grant (No. A-1547). ChatGPT was used during in preparation of the manuscript to improve the English writing.

References

- (1) Steidtner, J.; Pettinger, B. Tip-Enhanced Raman Spectroscopy and Microscopy on Single Dye Molecules with 15 Nm Resolution. *Phys. Rev. Lett.* **2008**, *100* (23), 236101. <https://doi.org/10.1103/PhysRevLett.100.236101>.
- (2) Bailo, E.; Deckert, V. Tip-Enhanced Raman Spectroscopy of Single RNA Strands: Towards a Novel Direct-Sequencing Method. *Angew Chem Int Ed* **2008**, *47* (9), 1658–1661. <https://doi.org/10.1002/anie.200704054>.
- (3) Zhang, R.; Zhang, Y.; Dong, Z. C.; Jiang, S.; Zhang, C.; Chen, L. G.; Zhang, L.; Liao, Y.; Aizpurua, J.; Luo, Y.; Yang, J. L.; Hou, J. G. Chemical Mapping of a Single Molecule by Plasmon-Enhanced Raman Scattering. *Nature* **2013**, *498* (7452), 82–86. <https://doi.org/10.1038/nature12151>.
- (4) Jiang, S.; Zhang, Y.; Zhang, R.; Hu, C.; Liao, M.; Luo, Y.; Yang, J.; Dong, Z.; Hou, J. G. Distinguishing Adjacent Molecules on a Surface Using Plasmon-Enhanced

- Raman Scattering. *Nature Nanotech* **2015**, *10* (10), 865–869. <https://doi.org/10.1038/nnano.2015.170>.
- (5) Domke, K. F.; Pettinger, B. Studying Surface Chemistry beyond the Diffraction Limit: 10 Years of TERS. *ChemPhysChem* **2010**, *11* (7), 1365–1373. <https://doi.org/10.1002/cphc.200900975>.
- (6) Lee, J.; Crampton, K. T.; Tallarida, N.; Apkarian, V. A. Visualizing Vibrational Normal Modes of a Single Molecule with Atomically Confined Light. *Nature* **2019**, *568* (7750), 78–82. <https://doi.org/10.1038/s41586-019-1059-9>.
- (7) Deckert, V.; Deckert-Gaudig, T.; Cialla-May, D.; Popp, J.; Zell, R.; Deinhard-Emmer, S.; Sokolov, A. V.; Yi, Z.; Scully, M. O. Laser Spectroscopic Technique for Direct Identification of a Single Virus I: FASTER CARS. *Proc. Natl. Acad. Sci. U.S.A.* **2020**, *117* (45), 27820–27824. <https://doi.org/10.1073/pnas.2013169117>.
- (8) Hambleton, S.; Tsuneda, A.; Currah, R. S. Comparative Morphology and Phylogenetic Placement of Two Microsclerotial Black Fungi from *Sphagnum*. *Mycologia* **2003**, *95* (5), 959–975. <https://doi.org/10.1080/15572536.2004.11833055>.
- (9) Eisenman, H. C.; Nosanchuk, J. D.; Webber, J. B. W.; Emerson, R. J.; Camesano, T. A.; Casadevall, A. Microstructure of Cell Wall-Associated Melanin in the Human Pathogenic Fungus *Cryptococcus Neoformans*. *Biochemistry* **2005**, *44* (10), 3683–3693. <https://doi.org/10.1021/bi047731m>.
- (10) Walker, C. A.; Gómez, B. L.; Mora-Montes, H. M.; Mackenzie, K. S.; Munro, C. A.; Brown, A. J. P.; Gow, N. A. R.; Kibbler, C. C.; Odds, F. C. Melanin Externalization in *Candida Albicans* Depends on Cell Wall Chitin Structures. *Eukaryot Cell* **2010**, *9* (9), 1329–1342. <https://doi.org/10.1128/EC.00051-10>.
- (11) Tsai, H.-F.; Chang, Y. C.; Washburn, R. G.; Wheeler, M. H.; Kwon-Chung, K. J. The Developmentally Regulated *Alb1* Gene of *Aspergillus Fumigatus*: Its Role in Modulation of Conidial Morphology and Virulence. *J Bacteriol* **1998**, *180* (12), 3031–3038. <https://doi.org/10.1128/JB.180.12.3031-3038.1998>.
- (12) Kumar, N.; Rae, A.; Roy, D. Accurate Measurement of Enhancement Factor in Tip-Enhanced Raman Spectroscopy through Elimination of Far-Field Artefacts. *Applied Physics Letters* **2014**, *104* (12), 123106. <https://doi.org/10.1063/1.4869184>.
- (13) Domke, K. F.; Zhang, D.; Pettinger, B. Toward Raman Fingerprints of Single Dye Molecules at Atomically Smooth Au(111). *J. Am. Chem. Soc.* **2006**, *128* (45), 14721–14727. <https://doi.org/10.1021/ja065820b>.
- (14) Gautam, I.; Singh, K.; Dickwella Widanage, M. C.; Yarava, J. R.; Wang, T. New Vision of Cell Walls in *Aspergillus Fumigatus* from Solid-State NMR Spectroscopy. *JoF* **2024**, *10* (3), 219. <https://doi.org/10.3390/jof10030219>.
- (15) Strycker, B. D.; Han, Z.; Bahari, A.; Pham, T.; Lin, X.; Shaw, B. D.; Sokolov, A. V.; Scully, M. O. Raman Characterization of Fungal DHN and DOPA Melanin Biosynthesis Pathways. *JoF* **2021**, *7* (10), 841. <https://doi.org/10.3390/jof7100841>.

- (16) Strycker, B. D.; Han, Z.; Duan, Z.; Commer, B.; Wang, K.; Shaw, B. D.; Sokolov, A. V.; Scully, M. O. Identification of Toxic Mold Species through Raman Spectroscopy of Fungal Conidia. *PLoS ONE* **2020**, *15* (11), e0242361. <https://doi.org/10.1371/journal.pone.0242361>.
- (17) Wang, H.; Liu, M.; Zhang, Y.; Zhao, H.; Lu, W.; Lin, T.; Zhang, P.; Zheng, D. Rapid Detection of *Aspergillus Flavus* and Quantitative Determination of Aflatoxin B1 in Grain Crops Using a Portable Raman Spectrometer Combined with Colloidal Au Nanoparticles. *Molecules* **2022**, *27* (16), 5280. <https://doi.org/10.3390/molecules27165280>.
- (18) Lofgren, L. A.; Ross, B. S.; Cramer, R. A.; Stajich, J. E. The Pan-Genome of *Aspergillus Fumigatus* Provides a High-Resolution View of Its Population Structure Revealing High Levels of Lineage-Specific Diversity Driven by Recombination. *PLoS Biol* **2022**, *20* (11), e3001890. <https://doi.org/10.1371/journal.pbio.3001890>.
- (19) Kim, W.-B.; Park, C.; Cho, S.-Y.; Chun, H.-S.; Lee, D.-G. Development of Multiplex Real-Time PCR for Rapid Identification and Quantitative Analysis of *Aspergillus* Species. *PLoS ONE* **2020**, *15* (3), e0229561. <https://doi.org/10.1371/journal.pone.0229561>.
- (20) Buil, J. B.; Zoll, J.; Verweij, P. E.; Melchers, W. J. G. Molecular Detection of Azole-Resistant *Aspergillus Fumigatus* in Clinical Samples. *Front. Microbiol.* **2018**, *9*, 515. <https://doi.org/10.3389/fmicb.2018.00515>.
- (21) Ortiz, S. C.; Pennington, K.; Thomson, D. D.; Bertuzzi, M. Novel Insights into *Aspergillus Fumigatus* Pathogenesis and Host Response from State-of-the-Art Imaging of Host–Pathogen Interactions during Infection. *JoF* **2022**, *8* (3), 264. <https://doi.org/10.3390/jof8030264>.
- (22) Han, Z. Raman Spectroscopy of Mold Conidia. Thesis, Texas A&M University. <https://hdl.handle.net/1969.1/198148>.
- (23) Carrion, S. D. J.; Leal, S. M.; Ghannoum, M. A.; Aimanianda, V.; Latgé, J.-P.; Pearlman, E. The RodA Hydrophobin on *Aspergillus Fumigatus* Spores Masks Dectin-1– and Dectin-2–Dependent Responses and Enhances Fungal Survival In Vivo. *The Journal of Immunology* **2013**, *191* (5), 2581–2588. <https://doi.org/10.4049/jimmunol.1300748>.
- (24) Rhodes, J. C. *Aspergillus Fumigatus* : Growth and Virulence. *Med Mycol* **2006**, *44* (s1), 77–81. <https://doi.org/10.1080/13693780600779419>.